Article

Eight-Element Antenna Array with Improved Radiation Performances for 5G Hand-Portable Devices

Atta Ullah [1], Naser Ojaroudi Parchin [2,*], Ahmed S. I. Amar [1,3] and Raed A. Abd-Alhameed [1,4]

1 Faculty of Engineering and Informatics, University of Bradford, Bradford BD7 1DP, UK
2 School of Engineering and the Built Environment, Edinburgh Napier University, Edinburgh EH10 5DT, UK
3 Air Defense College, Alexandria University, Alexandria 21568, Egypt
4 Department of Information and Communication Engineering, Basrah University College of Science and Technology, Basra 61004, Iraq
* Correspondence: n.ojaroudiparchin@napier.ac.uk

Abstract: This study aims to introduce a new phased array design with improved radiation properties for future cellular networks. The procedure of the array design is simple and has been accomplished on a low-cost substrate material while offering several interesting features with high performance. Its schematic involves eight air-filled slot-loop metal-ring elements with a 1×8 linear arrangement at the top edge of the 5G smartphone mainboard. Considering the entire board area, the proposed antenna elements occupy an extremely small area. The antenna elements cover the range of 21–23.5 GHz sub-mm-wave 5G bands. Due to the air-filled function in the configurations of the elements, low-loss and high-performance radiation properties are observed. In addition, the fundamental characteristics of the introduced array are insensitive to various types of substrates. Moreover, its radiation properties have been compared with conventional arrays and better results have been observed. The proposed array appears with a simple design, a low complexity profile, and its attractive broad impedance bandwidth, end-fire radiation mode, wide beam steering, high radiation coverage, and stable characteristics meet the needs of 5G applications in future cellular communications. Additionally, the smartphone array design offers sufficient efficiency when it comes to the appearance and integration of the user's components. Thus, it could be used in 5G hand-portable devices.

Keywords: 5G; beam steering; cellular networks; linear phased array; smartphone applications; substrate insensitive

1. Introduction

The current generation (4G) wireless cellular systems are not able to meet the demand for a high data-rate transfer for future communications [1]. Therefore, the 5th generation (5G) of mobile networks or wireless communications has been established to meet these challenges and provide several enhanced services on the internet of things (IoT), mobile broadband, massive multiple-input multiple-output (MIMO), machine-to-machine (M2M), and ultra-reliable communications [2–4]. The 5G spectrum is categorized in two broad regions as the Sub-6 GHz, ranging under 6 GHz frequency, and the millimeter-wave (mm-wave) region in which frequencies 24 GHz and above are adopted. In 5G networks, the mm-wave and sub-mm-wave spectrums play an important role in providing broadband communications that can support multiple sensing devices to demonstrate the performance of 5G service requirements [5–7]. Small antennas can be formed in linear or planar array schematics to overcome high attenuation and propagation losses and provide point-to-point communications. As represented in Figure 1, in the frequency range of 20–50 GHz, several candidate bands, such as 22.25, 26, 28, and 42 GHz, were determined by academia and industrial researchers to be considered efficient in 5G networks [8–12]. Apart from the cited frequencies, several bands (beyond 10 GHz), such as 15 and 21 GHz, were studied

for 5G applications [13–15]. It is also evident that compared with 4G, significant frequency shifting to the higher bands is expended for 5G communications.
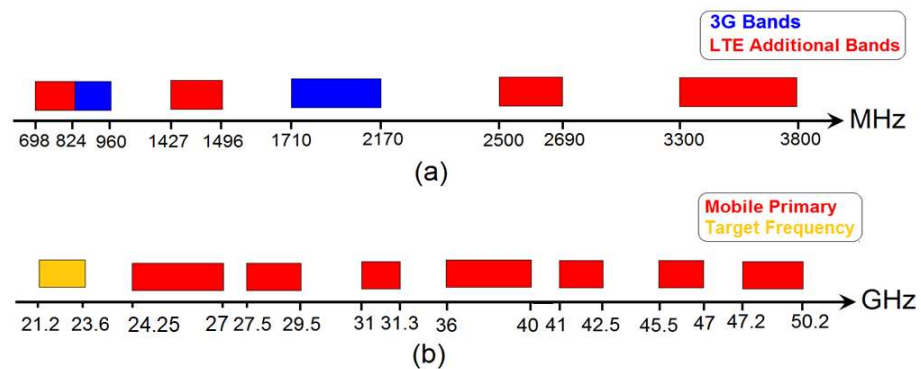

Figure 1. (**a**) Frequency spectra of 4G, (**b**) some candidate bands for 5G.

Linear phased arrays with compact resonators and broad frequency operation are desired for smartphone applications. Recently, several designs have been proposed to be integrated into handheld platforms [16–18]. One of the challenges in antenna design is to accomplish high-efficient antenna arrays which require careful consideration because it could increase the complexity of the design and material and implementation cost [19,20]. Therefore, in order to address these limitations and challenges, we introduce here a simple and straightforward design idea that can create high-efficiency and wide scanning radiations on a single substrate material and can be easily applied for smartphone applications. An additional selling point of the introduced design is its insensitivity to a wide range of substrate materials. In particular, this is due to the air-filled loop-ring resonators used as the radiation elements, which have a similar thickness to the FR4 substrate. Therefore, for different substrate types, the air acts as the main substrate and provides constant radiation properties with very low losses in terms of antenna gain and efficiency [21,22]. Unlike the reported design which needs a multi-layer configuration or complex feeding or high-cost materials, the proposed antenna array can be arranged on a single-layer cheap FR4 substrate and still provide sufficient radiations. The antenna elements can be easily fed using discrete or microstrip-line techniques. The presented antenna array is designed using the commercially available CST software package [23]. The array was manufactured on a standard smartphone board with FR4 material, and the properties of the single element have been experimentally measured. The design and fundamental characteristics of the single radiator and its phased array are elaborated below.

2. Antenna Design

The presented phased array is designed on a low-cost FR-4 dielectric with properties of h_{sub} = 0.8 mm, permittivity (ε_r) = 4.3, and loss tangent (δ) = 0.025. The schematic diagram of the design is represented in Figure 2. As depicted, eight elements of the air-filled/substrate-insensitive elements are adopted to form a 1×8 linear array at the edge of the smartphone board with an overall size of $W_{sub} \times L_{sub}$ = 55 $\times$ 110 mm^2. The employed linear array has a compact size of 8.5 $\times$ 43 mm^2. In order to obtain full radiation coverage in 5G mobile communication, another set of the presented phased array can be deployed at the bottom edge of the mainboard. The parameter values of the array design are specified in Table 1.
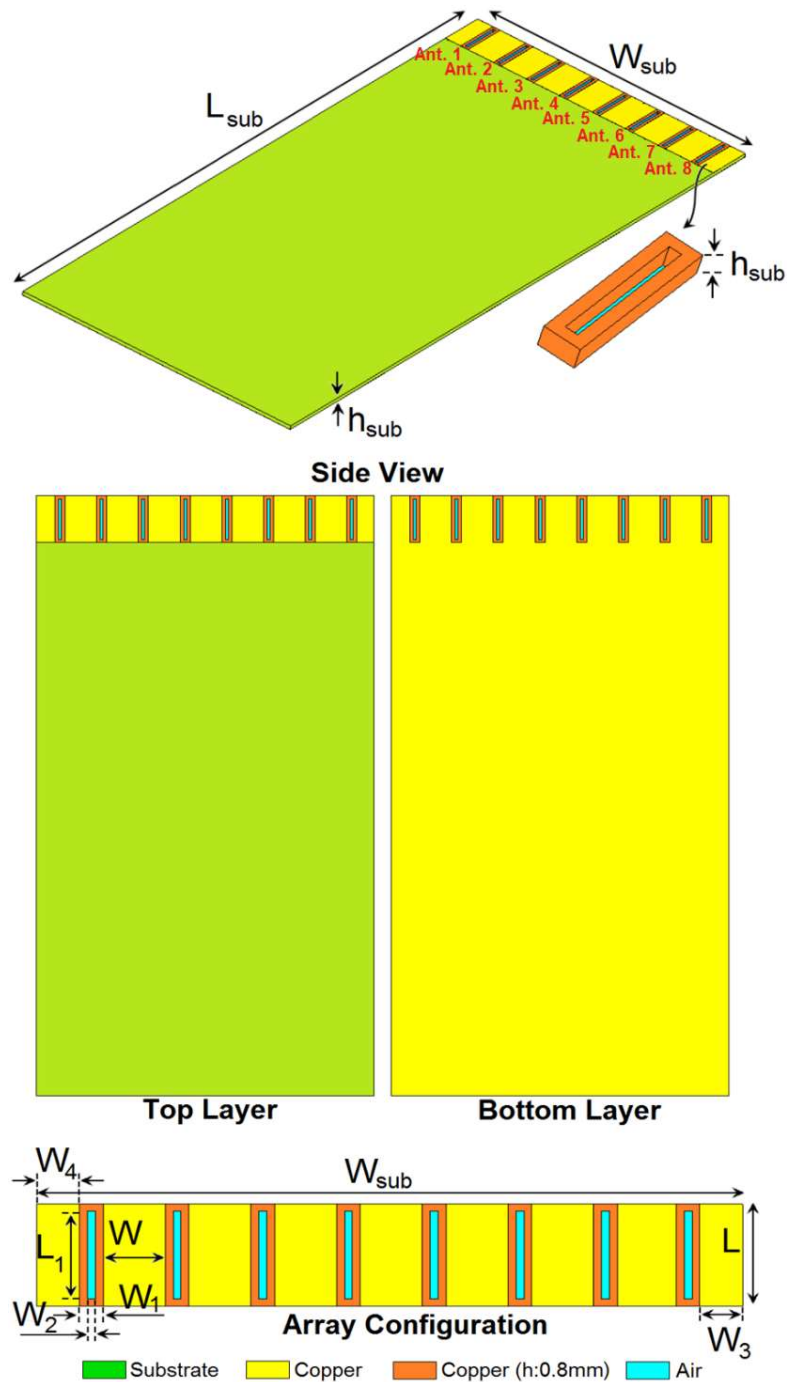
Figure 2. Details of the introduced array's configuration and design.

Table 1. Final dimensions of the 5G antenna parameters.

Parameter	W_{sub}	L_{sub}	h_{sub}	W	W_1
Value (mm)	55	110	0.787	5.25	1.5
Parameter	W_2	W_3	W_4	L	L_1
Value (mm)	0.5	3.125	3.125	8.3	7.8

Figure 3a depicts an ideal system architecture that can be used for a linear phased array antenna system. The feeding network of the phased array design is one of the critical issues to obtain a functional antenna array set. A 1 × 8 uniform linear array could be employed, on another thin substrate above the elements, for the presented array design.

It should be noted that each antenna radiator must be excited with equal magnitude and different phases [24,25]. The shape of the radiation beams can be defined by applying the relative phase amplitudes to each antenna radiator as below:

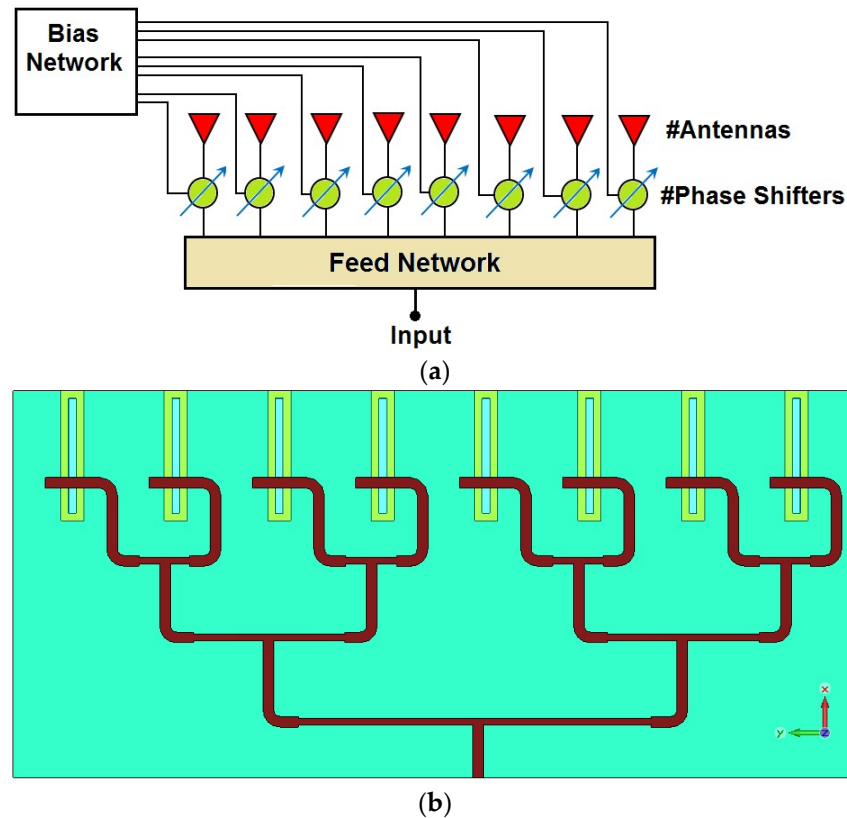$$\varphi = 2\pi \, (d/\lambda) \sin \theta \qquad (1)$$

Figure 3. (**a**) Phased array architecture and (**b**) typical 1:8 feed network for the array design.

There are various techniques of feed network design for this purpose: parallel (Figure 3b), series, etc. The power dividers (such as Wilkinson) divide the power equally 1: N and also unequally by changing the input and output [26]. In general, in the microstrip-line power dividers, the number of junctions from the input to each output is controlled for tapering amplitude. Moreover, the overall performance of the power divider mainly depends on the power-split level for each output; therefore, the design process can be simple, and the fabrication sensitivity can be insignificant [27].

3. Single-Element Antenna

In general, the microstrip printed slot antenna is a resonator that can be easily formed by cutting a thin slot in a metal-sheet plane. Its size is a half-wavelength ($\lambda/2$) of the antenna operation frequency [28–30]. It can exhibit different polarizations (vertical/circular/horizontal polarizations) depending on its placement, feeding, and antenna configuration. This work has been started by designing a typical slot antenna operation at 21–23.5 GHz. In this study, a rectangular slot radiator is converted into a rectangular metal-ring radiator of the same thickness as the substrate in order to improve the radiation performance and eliminate the impact of high-loss FR-4 dielectric (h_{sub}). The design evaluation and structures of the conventional slot and rectangular metal-ring antennas are depicted in Figure 4a,b. It can be also observed that the discrete feeding technique is employed to feed the radiator in the simulations.
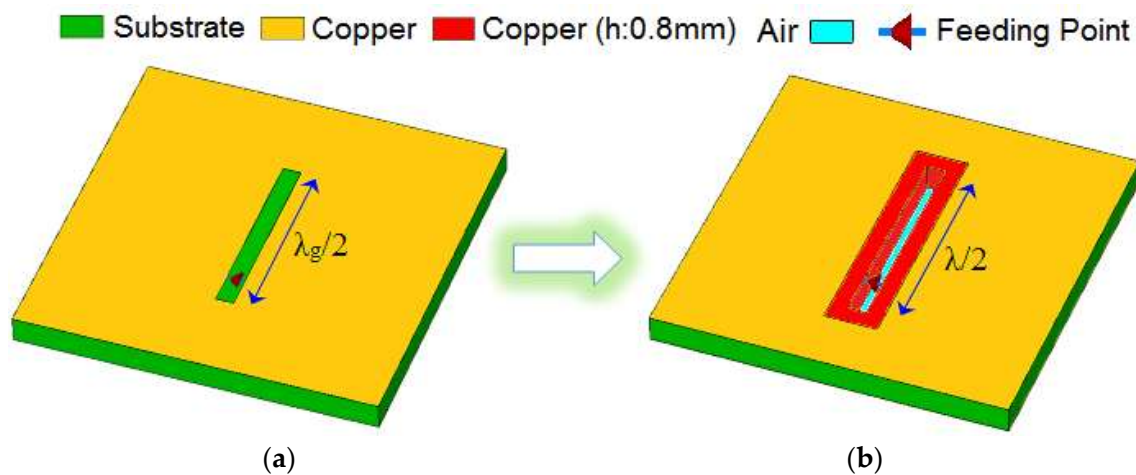
Figure 4. (**a**) Conventional $\lambda/2$ slot resonator and (**b**) the configuration of the proposed metal-ring/air-filled slot.

As shown in Figure 5, the proposed design is flexible and by changing the size of the main radiator (L_1), the antenna operating frequency can be easily tuned to the desired band. Figure 6a plots the distributions and densities of the surface currents at the resonating frequency in the top and back layers of the suggested antenna, respectively. It can be observed that the currents are significantly distributed around the slot resonator. Moreover, the embedded metal-ring loop appeared highly active with the surface currents flowing around it. The 3D radiation of the introduced design has been plotted in Figure 6b. Observations have shown that the metal-ring/air-filled resonator provided good radiation, supporting substrate sides at the top and bottom. Moreover, the element provides a high gain level of 5 dB at 22.25 GHz. Furthermore, it is worth mentioning that the -0.35 and -0.38 (radiation and total) efficiencies are discovered for the element at the resonating frequency.
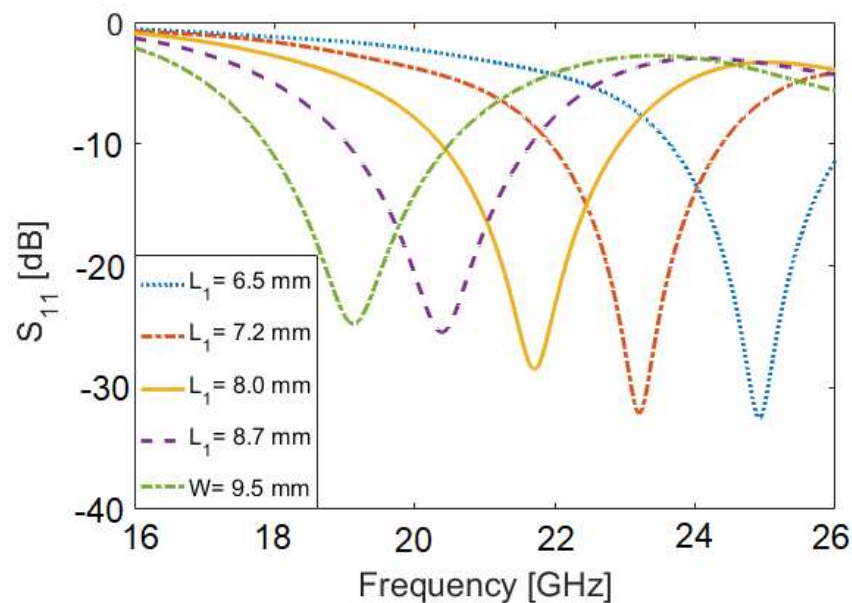

Figure 5. Operation-frequency tuning of the designed antenna for different lengths of the slot resonator.
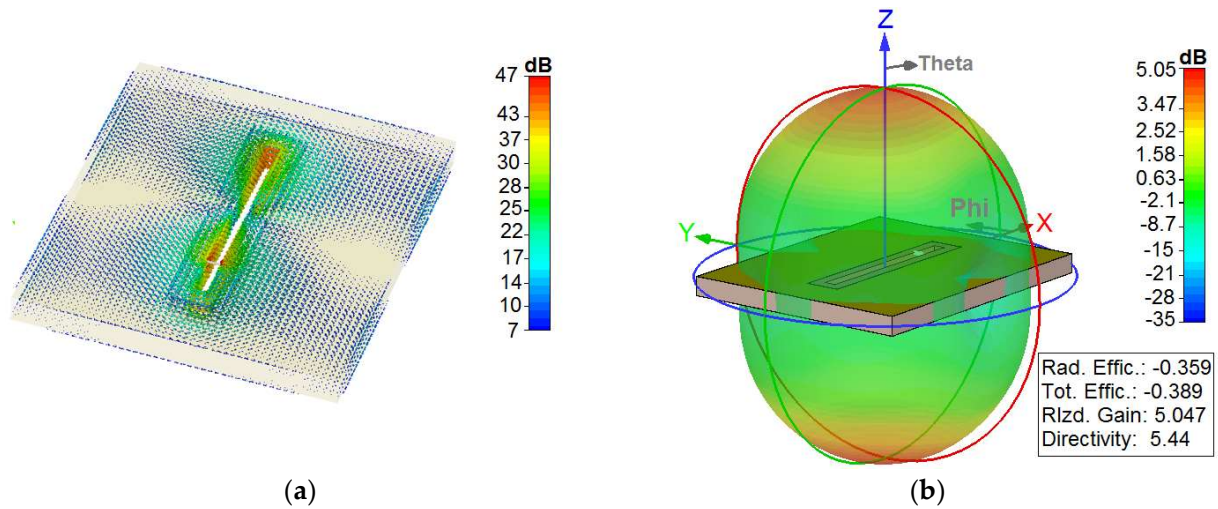
(**a**)　　　　　　　　　　　　　　　　　　　　　　　　　　(**b**)

Figure 6. (**a**) The current densities and (**b**) radiation at 22.25 GHz.

4. Characteristics of the 5G Smartphone Antenna Array

This section describes and examines the main properties and radiation parameters of the represented array and its beam-tuning capabilities. The S parameters ($S_{11} \sim S_{81}$) of the introduced linear array design are represented in Figure 7. As shown, the design offers 2.5 GHz operational bandwidth with a single resonance at 22.5 GHz, and with lower than −17 dB couplings of the slot radiators. The current distribution at 22.25 GHz is plotted in Figure 8. As can be observed, the currents have mainly concentrated on the top portion of the mainboard. It can be seen that the employed metal-ring radiator is very active and the current flows are mainly distributed around them [31,32].
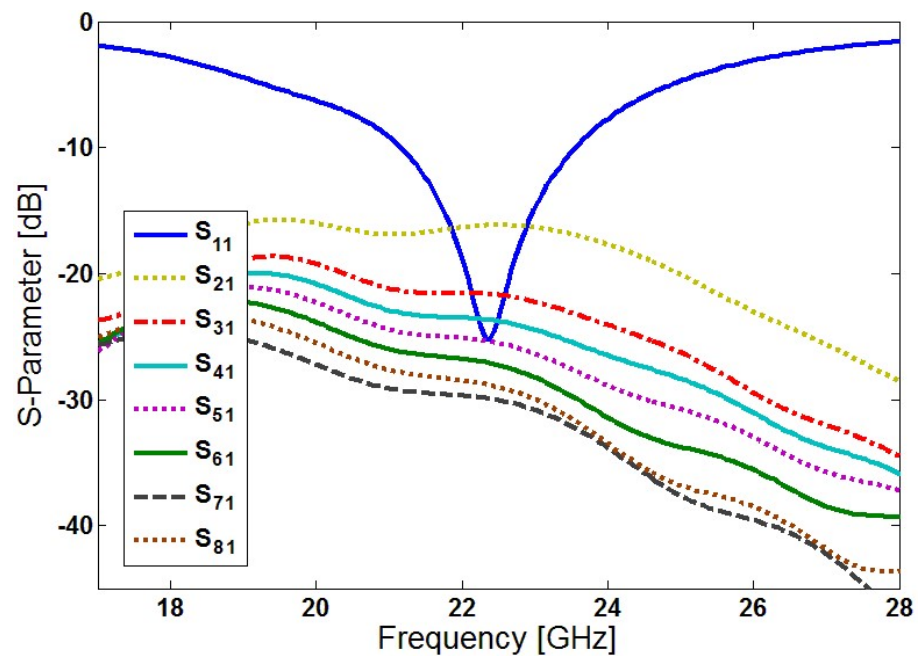

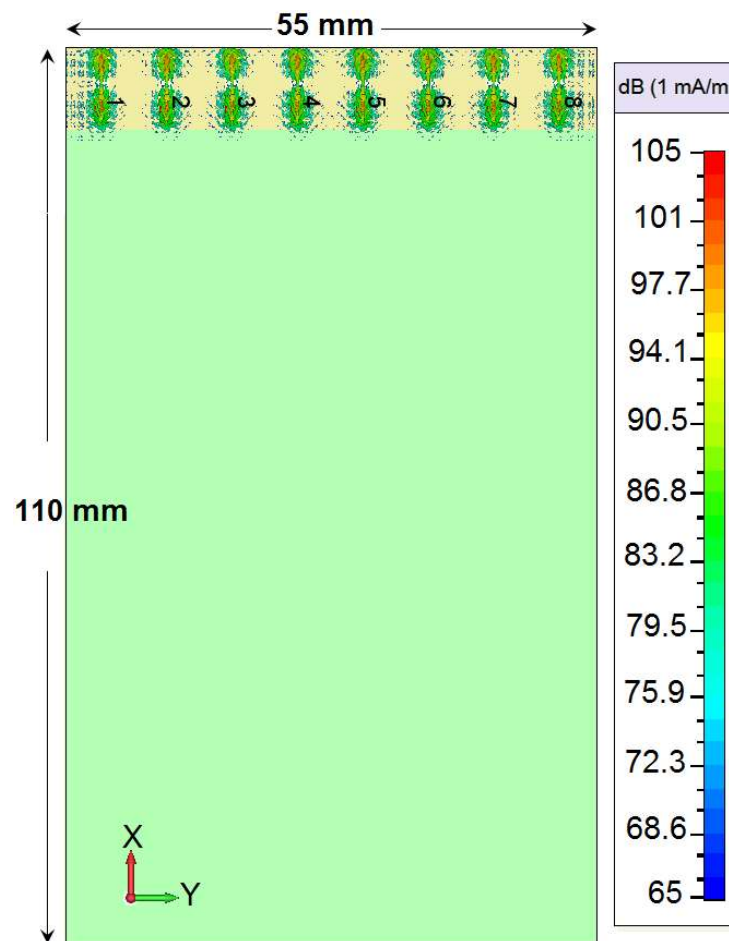**Figure 7.** S parameters for the proposed phased array.

Figure 8. Current distribution at 22.25 GHz for 0° beam of the phased array.

Figure 9 shows the 3D beams of the introduced array radiations for various tuning angles at 22.25 GHz. As can be noticed, the array beams exhibit a wide scanning property over 0°–70°. On the other hand, we observe well-defined end-fire radiations and quite sufficient gains and directivity over the scanning angles. As represented, the array offers an end-fire radiation mode at the selected scanning angle (0°, 15°, 30°, 45°, 60°, and 70°) which could provide half-space radiation coverage with point-to-point scanning possibility at a different desired angle. As mentioned earlier, to acquire full radiation coverage, another set of the introduced antenna can be located at the bottom side of the mainboard PCB.

Figure 10 shows the simulated 2D-cartesian gain levels of the suggested array beam steering at minus/plus scanning angles. It is shown that the antenna provides wide scan and high-gain beam steering. At 0° to ±50° scannings, the array gains are almost constant and offer greater than 11 dB gains. The critical characteristics of the design radiations, such as the directivities and efficiencies for the various radiation beams of the suggested smartphone array at 22.25 GHz, have been represented in Figure 11. Across the range of 0°–60°, the array efficiencies are greater than 90%. In addition, for the angles below ±50, the directivity value varies from 10 to 12 dBi. The efficiency characteristics of the introduced array in the operating frequency range at the 0^0 scanning angle are plotted in Figure 12. It is discovered that the designed 5G smartphone antenna provides good efficiencies over the frequency band. As represented, a more than −0.15 (97%) radiation efficiency and −1 (80%) total efficiencies have been achieved for the array at the operation band of 21–23.5 GHz. Moreover, the design exhibits sufficient gain values over the targeted frequency band. It was realized that the maximum gain improves while moving to the higher frequencies.
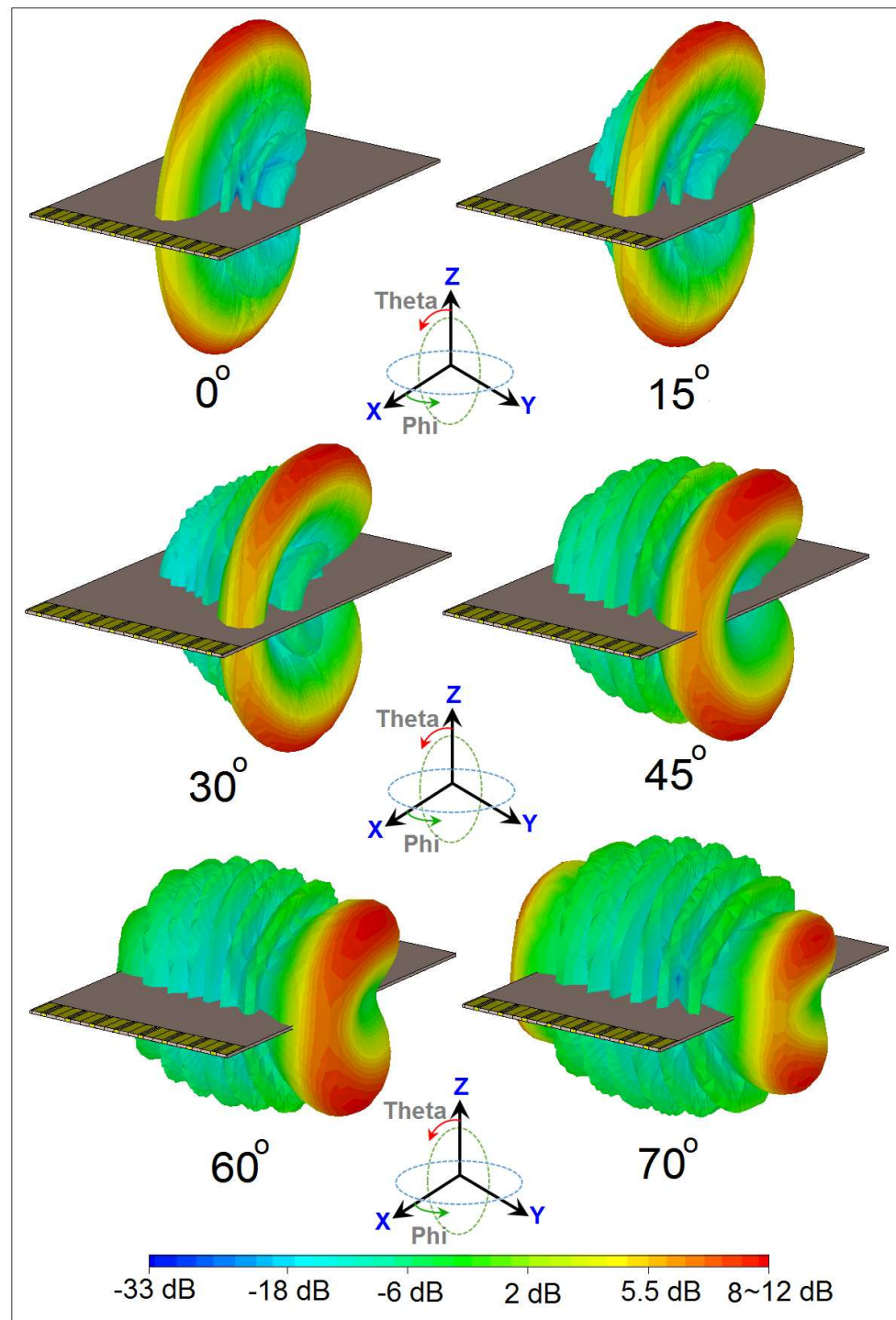
Figure 9. Transparent views of the array beams.
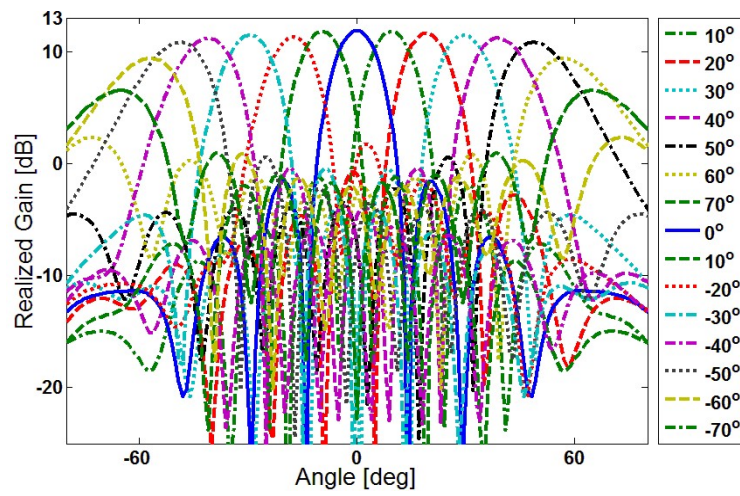
Figure 10. Array gain levels for the scanning radiation beams.
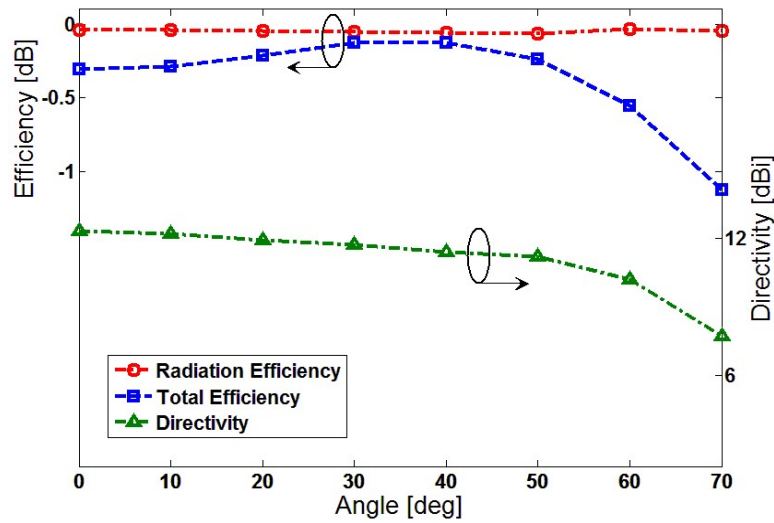

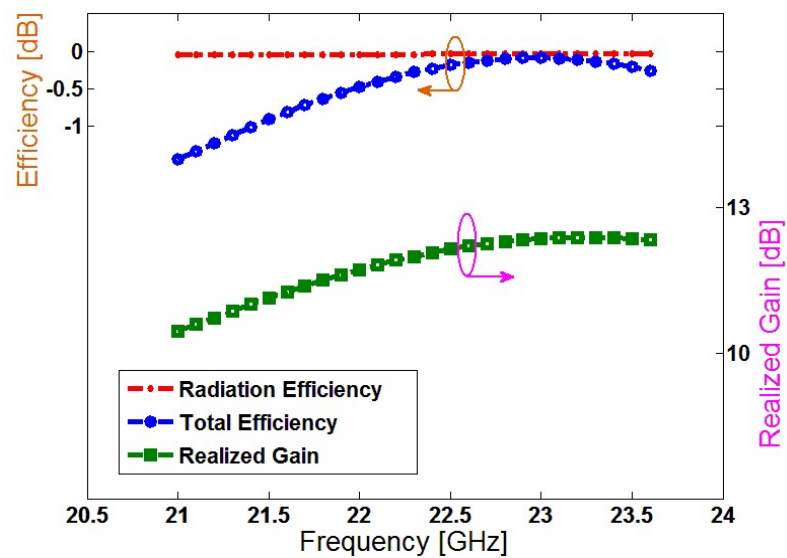**Figure 11.** Simulated fundamental radiation parameters at 22.25 GHz.

Figure 12. Fundamental radiation parameters over the array impedance bandwidth.

5. Comparison of the Proposed Design with the Conventional Arrays

In order to clarify the improved and higher performance of the introduced phased array compared with the conventional arrays (such as patch and slot antenna arrays), the main properties have been compared and discussed in this section. All designed arrays with eight resonators and a distance of 6.75 mm (λ/2) are placed in identical smartphone mainboards with FR4 substrate materials to operate at the target frequency of 22.25 GHz. The radiations, beam steering, S parameters, and efficiencies are studied. Figure 13 illustrates the schematics of the cited 5G array antennas.
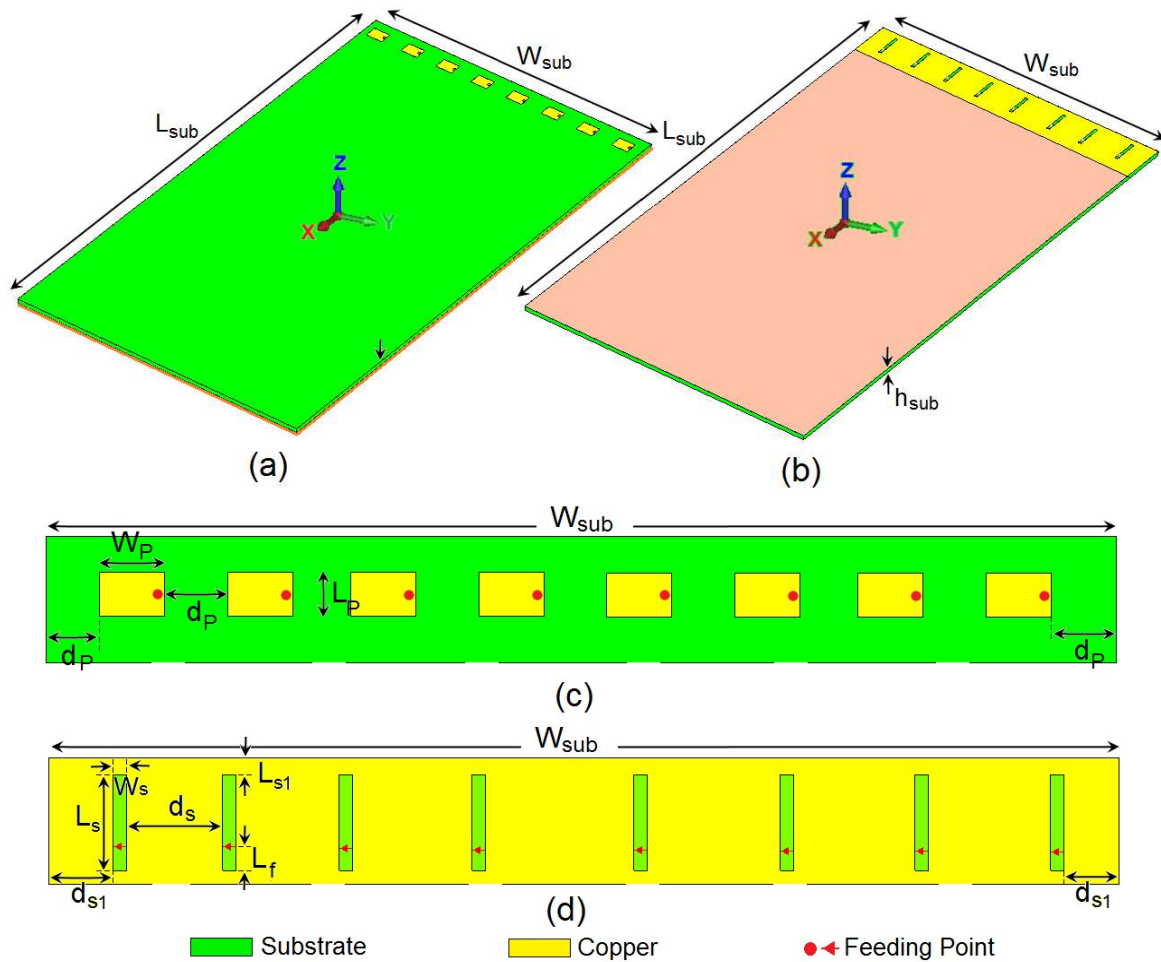
Figure 13. Side views of the smartphone mainboard with conventional (**a**) patch and (**c**) slot array antenna, (**b**) the detailed (**c**) patch, and (**d**) slot array arrangements.

Both conventional arrays have been designed to resonate at 22 GHz. Figure 14 depicts their S parameters. As shown, the antennas exhibit good behavior with sufficient couplings. Compared with the S parameters of the proposed design (in Figure 7), the conventional arrays provide sufficient and almost similar S-parameter results. Therefore, they can be good candidates for radiation comparison. Figure 15 compares the radiation efficiency of the designed arrays for various angles of 0° to 60°. It can be seen that compared with the conventional slot and patch array, the introduced array offers very high efficiency. It should be noted that using $x = 10\log_{10}k$, the percentage (linear) value of the antenna efficiency can be converted to dB (logarithmic) [33]. Therefore, as clearly observed, even though the proposed antenna is designed on a lossy substrate (FR4), it offers a much higher efficiency (almost 100%) compared to the conventional designs (80–85%). This is mainly due to the employed design technique which eliminates the loss of the substrate material.
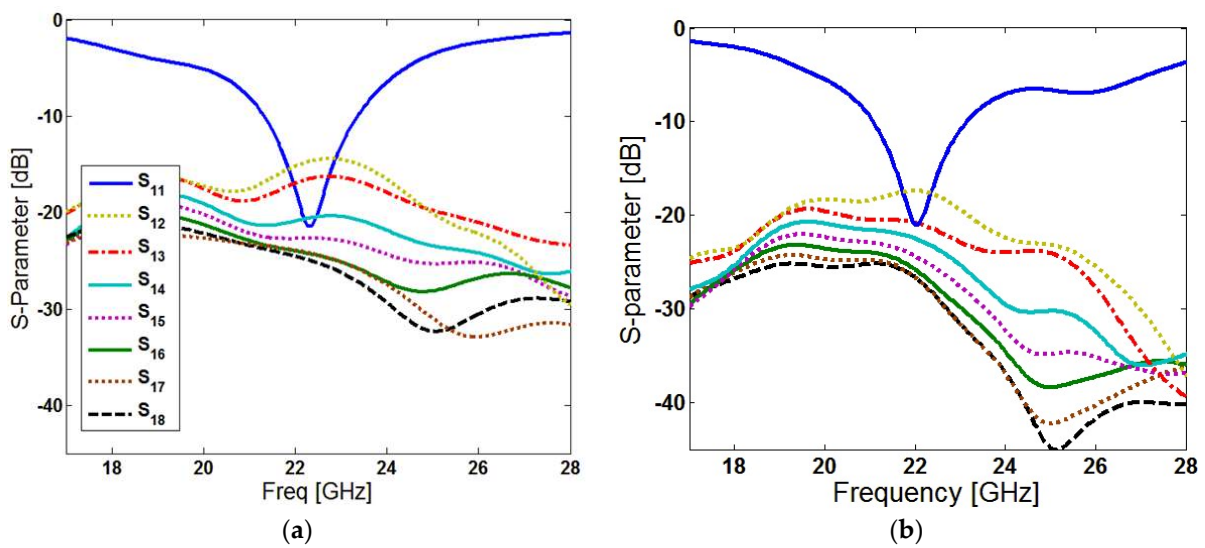
Figure 14. S parameters of the conventional array antennas, (**a**) slot antenna and (**b**) patch antenna.
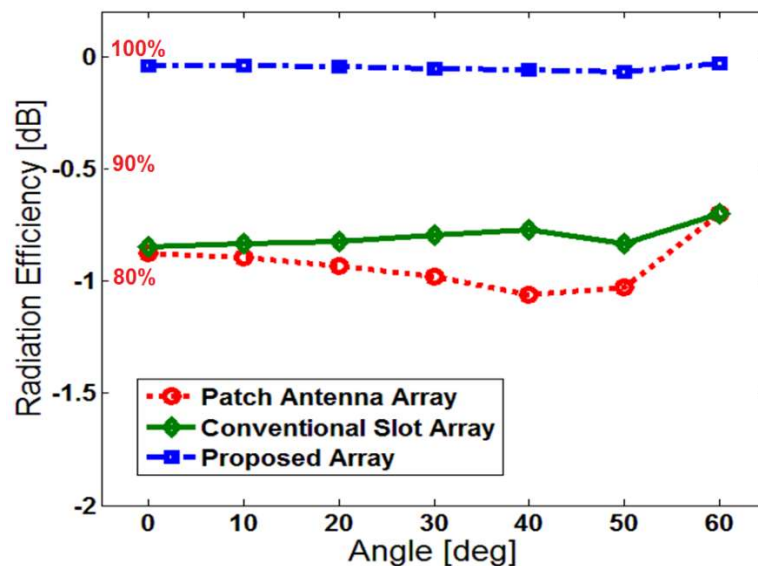

Figure 15. Comparison between the radiation efficiencies of the arrays illustrated in Figure 12 and the proposed design.

Figure 16 plots and compares the 3D beam-steering radiations of the selected antenna arrays with gain levels in the range of 0–60 degrees. As represented, compared with the conventional antenna arrays [Figure 16a,b], the suggested array design offers improved and almost constant radiation gains at various degrees. The simulations and efficiency/gain calculations for each radiation beam were carried out using computer simulation technology (CST) software. As shown, the efficiency values of the proposed design are better than −0.5 dB (90%), while for the conventional design, the parameter is less than −1 dB (80%). In addition, higher efficiency results are discovered for the proposed design. Despite the fact that the conventional patch antenna is higher at 0 degrees, when moving the scanning to higher levels, both conventional arrays (patch and slot) have significantly lower gain levels. Moreover, for the patch array placed at the top side of the mainboard, the radiation coverage will be limited, and achieving full coverage would be challenging. Meanwhile, as shown in Figure 16c, the introduced array design generates end-fire beams with increased radiation coverage. Therefore, using the proposed design technique and applying the

air-filled metal resonators, the antenna's critical properties can be improved for better communications [34,35].
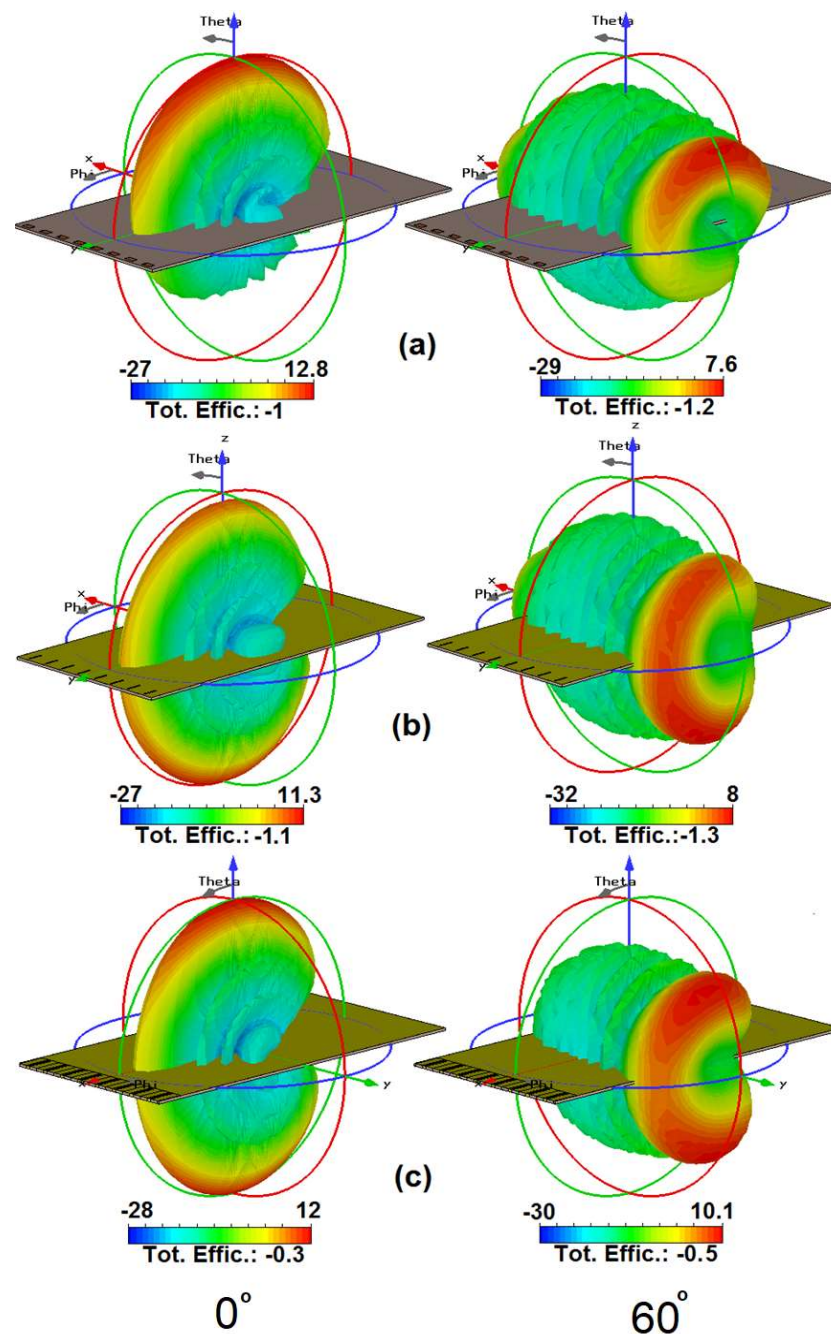
Figure 16. Three-dimensional radiation beams of the antennas are shown in Figure 8 and the proposed design.

6. Insensitivity Function of the Proposed Array Design

As mentioned above, the fundamental properties of the introduced array design are insensitive to different substrate characteristics. The properties of the dielectric substrate, including the permittivity and loss tangent, are critical parameters to control the radiation and performance of the small antennas. In order to clarify this property, the array coefficient reflection (S_{nn}) for various dielectric constant (ε_r) values are studied in Figure 17. For the conventional slot antenna array plotted in Figure 13b, when the value of the antenna permittivity (ε_r) increases from 2 to 6, the resonating frequency of the conventional slot

antenna (S_{11}) decreases from 28 to 18 GHz. However, as can be observed from Figure 17, unlike the conventional array design, the introduced air-filled array offers similar S_{11} results for various values of the substrate permittivity. From this result, it can be concluded that the array design is insensitive, and its reflection coefficient remains constant for various types of substrates.
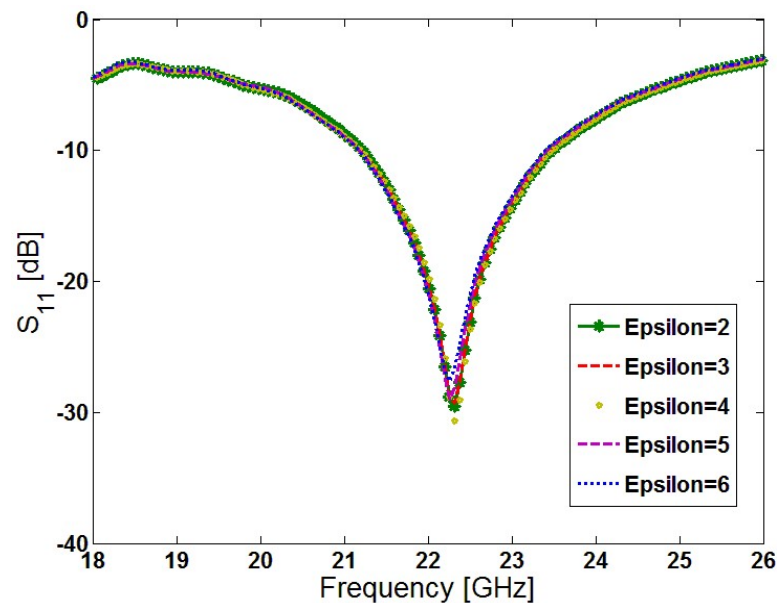

Figure 17. S_{11} results of the array for various values of Epsilon (ε_r).

The loss tangent (δ) is another substrate characteristic that should be considered for the insensitivity function of the proposed array design [36]. It plays a vital role and can affect both the cost and radiation characteristics of an antenna design. The fundamental radiation properties of the introduced array design, including the realized gain, radiation, and efficiencies at different scanning degrees at 22.25 GHz of the presented array design for various loss tangent values, are illustrated in Figure 18. The studied loss tangent varies from 0.005 to 0.5. As shown, changing the value of δ does not affect the radiation properties of the phased array. The design exhibits similar behavior with high efficiencies. It can be found that the designed phased array offers almost the same values of efficiencies (radiation and total) and very insignificant variation. In addition, at different degrees, the gain characteristic of the introduced array does not change. The radiation characteristics of the introduced design with various lengths of the ground plane have been studied in Figure 19. As illustrated, as the array elements are the insensitive slot-loop radiators with the air substrates, the ground-plane impact on the array performance is insignificant. However, as can be seen, using different lengths for the ground plane, different values of the fundamental radiation properties can be obtained.

Table 2 exhibits a comparative summary of the antenna characteristics for the proposed design with the recently reported smartphone 5G phased arrays available in the literature [37–45]. As depicted in the table, the suggested design can support wide scanning angles with better gain and efficiency characteristics. In addition, different from the reported designs, the gain and efficiency characteristics of the design are almost constant over the main scanning angles (0–60 degrees). In addition, the antenna elements have more than 17 dB isolation. Furthermore, unlike the reported design, the proposed antenna is insensitive to different substrate materials which is a unique function and can be demonstrated in low-cost substrates. Its performance is also almost constant for different ground-plane lengths as discussed in Figure 19.
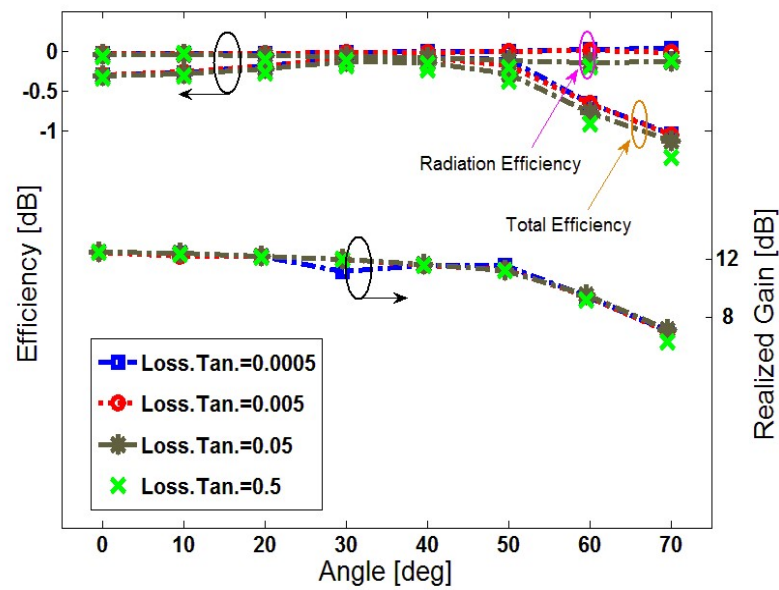
Figure 18. Efficiencies and gain results for different loss tangents (δ) at 22.25 GHz for different scanning angles.
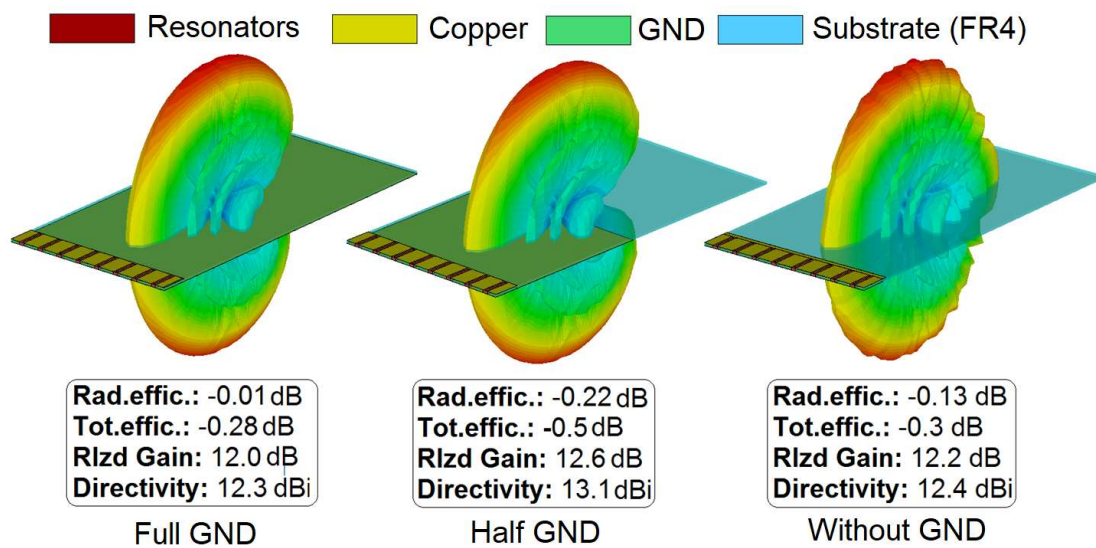
Figure 19. Fundamental radiation properties of the antenna with different sizes of the ground plane.

Table 2. Comparison between the proposed and the reported mobile handset antennas.

Reference	Bandwidth (GHz)	Efficiency (%)	Gain (dB)	Isolation (dB)	Scanning Range	Insensitivity Function
[37]	21–22	-	8–12	14	0°~75°	No
[38]	27.5–28.5	70	7–11	11	0°~60°	No
[39]	21–23	85	9–11.5	12	0°~60°	No
[40]	27.4–28.8	-	7–11	16	0°~60°	No
[41]	27–29	80	5–9.5	13	0°~75°	No
[42]	27.5–28.5	-	8–11.5	15	0°~60°	No
[43]	27.75–28.25	-	10–13	20	0°~50°	No
[44]	25–29	75–90	8–11	15	0°~75°	No
[45]	27.5–29.5	-	6–8	20	0°~30°	No
Proposed	21–23.5	80–95	10–12.5	17	0°~75°	YES

7. Fabricated Prototype and Experimental Results

The proposed substrate-insensitive phased array was fabricated in a standard FR-4 dielectric. Figure 20a shows the front/back views of the prototype sample. During the fabrication process, eight-slot holes with a distance of $\lambda/2$ have been made to hold the metal-ring resonators. In the next step, the metal-ring resonators were made separately and then inserted into the slot holes on the PCB. Due to some restrictions in terms of equipment and also due to the fact that the antenna elements exhibit almost identical frequency/radiation behavior, the S_{11} and radiation pattern of one antenna element placed at the corner is measured for the introduced phased array.

(**a**)
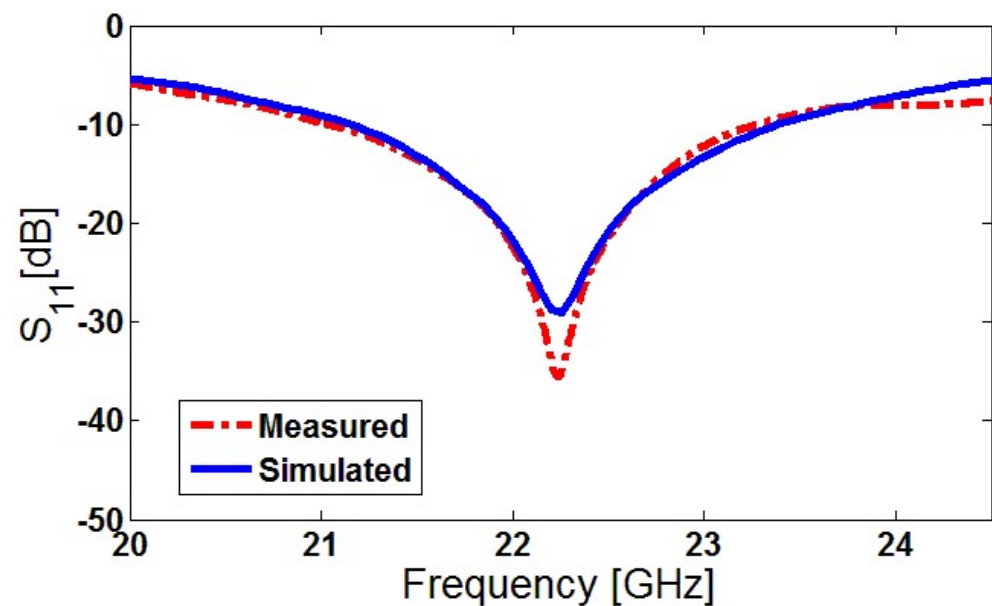
(**b**)

Figure 20. (**a**) Fabricated prototype sample with the coaxial feeding mechanism of the element and (**b**) measured/simulated comparison for the antenna reflection coefficient (S_{11}).

However, it should be noted that the mutual coupling effects are not considered in this experimental approach. As can be observed from Figure 20a, in order to measure the S_{11} characteristic of the single-element resonator, the inner conductor of a coaxial cable was extended across the ring resonator and soldered on the PCB ground plane. The simulated/measured S_{11} results of the single-element radiator placed on the mainboard are also plotted and compared in Figure 20b. As evident from the figure, the antenna element exhibits a sufficient measured/simulated S_{11}. In addition, a good agreement is observed between the experimental and simulation results. It is worth mentioning that due to the flexibility of the employed feeding method and also in order to acquire the best possible measured result and also eliminate the SMA connector/cable losses, the feeding point of the antenna element can be slightly adjusted to obtain a better result.

The radiation patterns (including the E and H planes) of the single-element antenna are also measured. Figure 21a plots the measured 2D polar patterns for the element under experiment. As shown, the single-resonator exhibits a quasi omnidirectional radiation shape in the E-plane, while in the H-plane, the radiation's main direction ended in the end-fire mode. Furthermore, in order to study the beam-steering potential of the proposed design with a general perspective, using the measured radiation data of the single antenna, the beam patterns of the introduced array have been synthesized and simulated [46]. The calculated results in the scanning range of 0°~70° were illustrated in Figure 21b. As can be observed, a well-defined beam-steering function is obtained for the synthesized beams in the range from 0° to 70°. It is worth mentioning that in the realist approach (where all the elements are measured and mutual couplings and phase shifting are included), the obtained results might be slightly different.
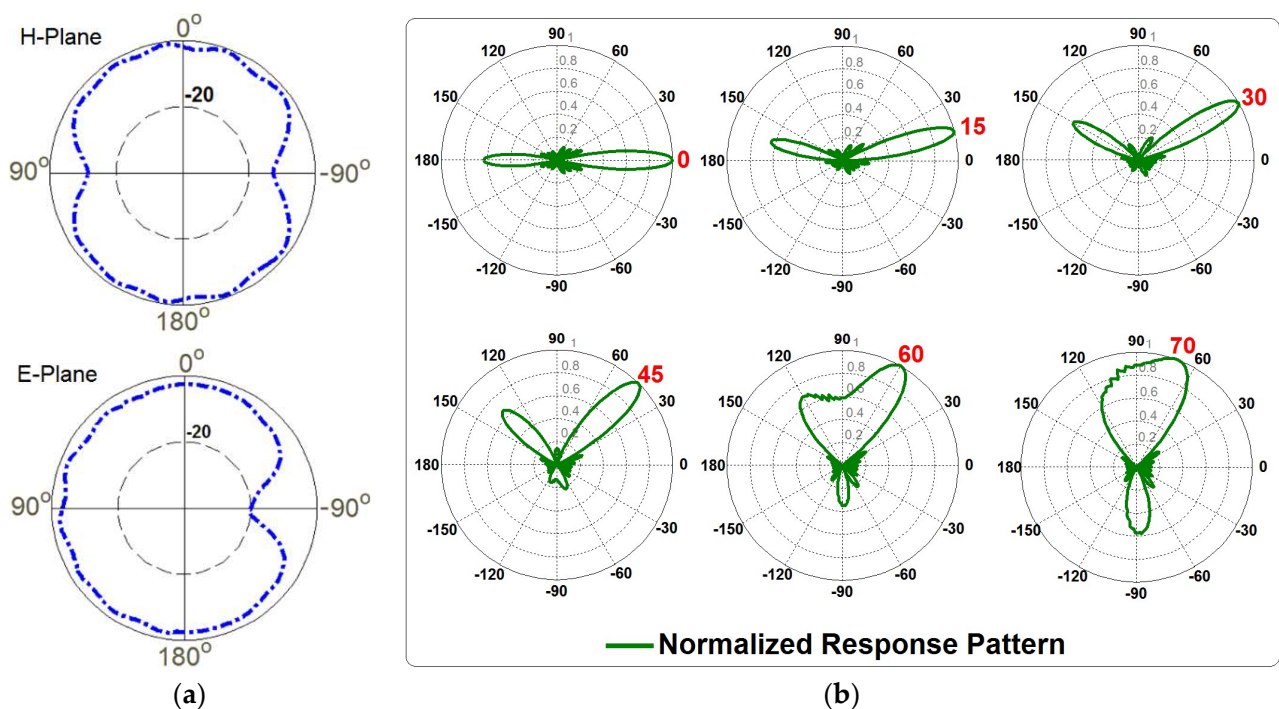
Figure 21. (**a**) Measured radiation patterns and (**b**) synthesized array beams using the single-element experiments.

8. Effect of User Hand in Data-Mode

The user-hand effect is a critical part of smartphone applications on handheld platforms and usually creates negative impacts on the radiation and properties of the smartphone antennas [47–50]. This section studied and compared the radiation beams, antenna gain, and efficiencies of the introduced array in the appurtenance of the user hand for the Data-Mode scenario. Figure 22 represents the array beams at different scanning degrees

(0°~75°). It is clearly shown that the introduced array design offers well-defined radiations with sufficient gains and radiation coverage in quasi-end-fire radiation mode. However, as mentioned before, due to the negative impact of the user-hand phantom, a slight reduction in the array performance was observed. Figure 23 illustrates and compares the losses of the performances of the phased array design in terms of the realized gain and efficiencies in the Data-Mode (DM) compared with Free-Space (FS). As seen, the total losses of the designed array parameters for the antenna gain are around 0.5 to 1.5 dB. In addition, in the scanning range of 0° to 50°, the efficiency reduction is less than 0.25 dB (5%). However, as expected, by moving to the higher scanning angles (60°~70°), an about 15–20% reduction is observed in the antenna efficiency. Therefore, it can be concluded that the effect of the user's hand is not significant.
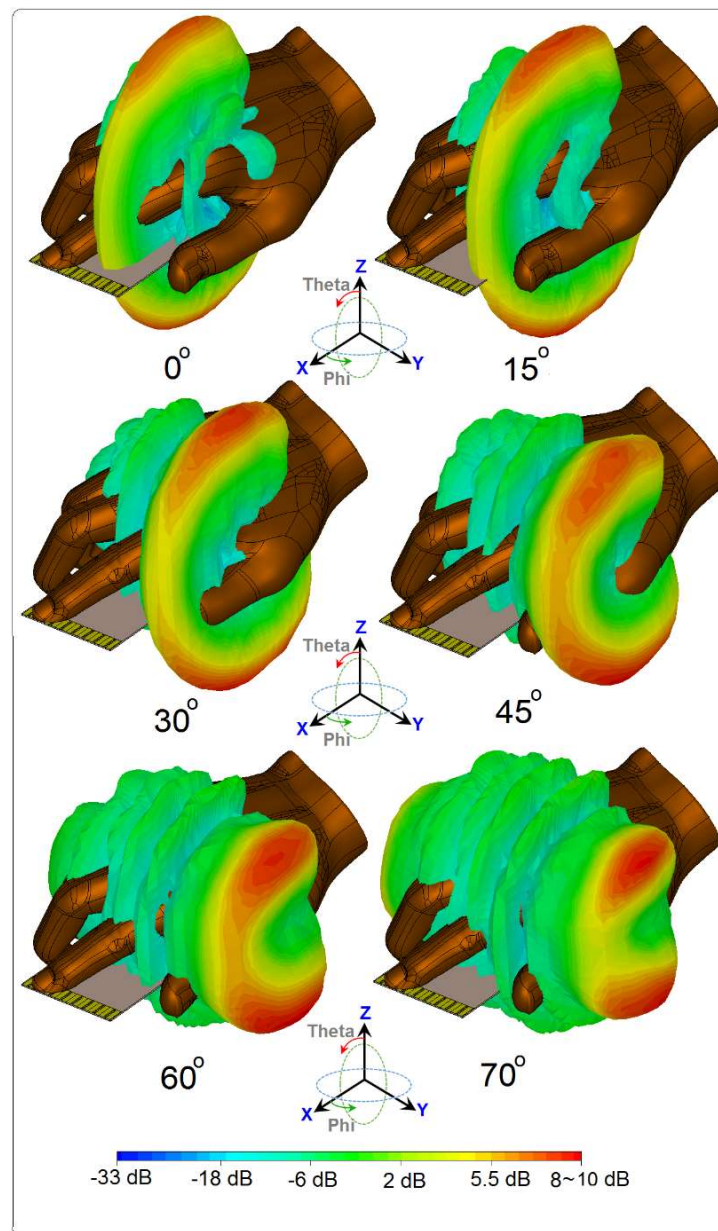

Figure 22. Three-dimensional beams of the array radiation in Data-Mode.
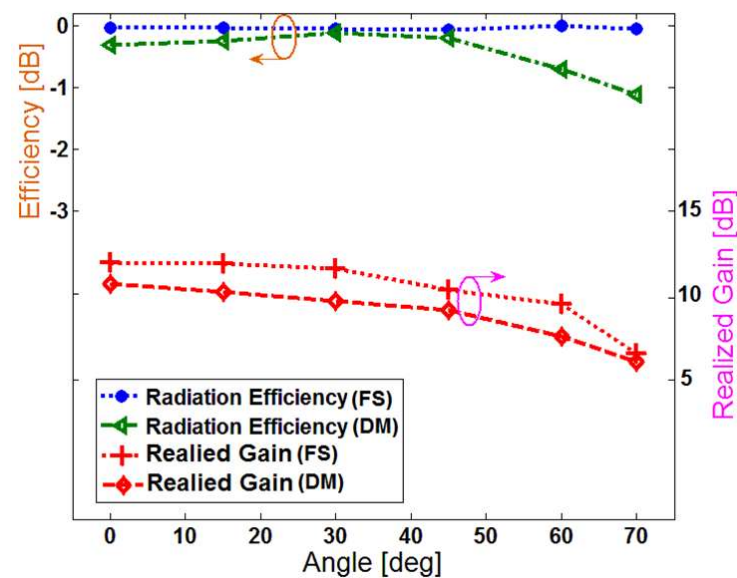
Figure 23. Comparison between the characteristics of the array in FS and DM.

9. Conclusions

This manuscript proposes a new beam-steerable array antenna design with improved performance and substrate insensitivity for modern 5G smartphones. The antenna array is designed on the FR-4 dielectric and its configuration contains eight slot-loop/metal-ring resonators with the air-filled substrate in a 1 × 8 array form located at the edge of the smartphone board. The usefulness of the introduced array for 5G applications is validated through simulations and measurements. The proposed design provides a wide impedance bandwidth of 21–23.5 GHz. It also exhibits constant radiation properties with very low losses in terms of the antenna gain, S parameters, and efficiency for different substrate materials. It also offers high gains and efficiencies at frequencies different from its operating band. In addition, sufficient radiation is observed in the presence of the user's hand in Data-Mode. Considering these advantages, the array is highly suitable for modern 5G smartphones.

Author Contributions: Writing—original draft preparation, A.U., N.O.P. and R.A.A.-A.; writing—review and editing, N.O.P., A.S.I.A. and R.A.A.-A.; investigation, N.O.P. and A.U.; resources, N.O.P. and A.S.I.A.; for other cases, all authors have participated. All authors have read and agreed to the published version of the manuscript.

Data Availability Statement: All the data have been included in the study.

Conflicts of Interest: The authors declare no conflict of interest.

References

1. Gupta, P. Evolvement of mobile generations: 1G to 5G. *Int. J. Technol. Res. Eng.* **2013**, *1*, 152–157.
2. Rappaport, T.S.; Sun, S.; Mayzus, R.; Zhao, H.; Azar, Y.; Wang, K.; Wong, G.N.; Schulz, J.K.; Samimi, M.; Gutierrez, F. Millimeter wave mobile communications for 5G cellular: It will work! *IEEE Access* **2013**, *1*, 335–349. [CrossRef]
3. Rappaport, T.S.; Gutierrez, F.; Ben-Dor, E.; Murdock, J.N.; Qiao, Y.; Tamir, J.I. Broadband millimeter-wave propagation measurements and models using adaptive-beam antennas for outdoor urban cellular communications. *IEEE Trans. Antennas Propag.* **2013**, *61*, 1850–1859. [CrossRef]
4. Liu, D.; Pfeiffer, U.; Grzyb, J.; Gaucher, B. *Advanced Millimeter-Wave Technologies*; John Wiley and Sons: Hoboken, NJ, USA, 2009.
5. Yarali, A. Fifth Generation (5G) Cellular Technology. In *Public Safety Networks from LTE to 5G*; Wiley: Hoboken, NJ, USA, 2020; pp. 171–188.
6. Narayan, C.P. *Antennas and Propagation*; Technical Publications: Pune, Maharashtra, India, 2007.

7. Roh, W.; Seol, J.-Y.; Park, J.; Lee, B.; Lee, J.; Kim, Y.; Cho, J.; Cheun, K.; Aryanfar, F. Millimeter-wave beamforming as an enabling technology for 5G cellular communications: Theoretical feasibility and prototype results. *IEEE Commun. Mag.* **2014**, *52*, 106–113. [CrossRef]

8. Rajagopal, S.; Abu-Surra, S.; Pi, Z.; Khan, F. Antenna array design for multi-gbps mmwave mobile broadband communication. In Proceedings of the 2011 IEEE Global Telecommunications Conference—GLOBECOM 2011, Houston, TX, USA, 5–9 December 2011; pp. 1–6.

9. Siddiqui, Z.; Sonkki, M.; Chen, J.; Berg, M.; Leinonen, M.E.; Pärssinen, A. Dual-band dual-polarized antenna for mm-wave 5G base station antenna array. In Proceedings of the 2020 14th European Conference on Antennas and Propagation (EuCAP), Copenhagen, Denmark, 15–20 March 2020; pp. 1–4.

10. Parchin, N.O.; Abdalhameed, R.A. A compact Vivaldi antenna array for 5G channel sounding applications. In Proceedings of the 12th European Conference on Antennas and Propagation (EuCAP 2018), London, UK, 9–13 April 2018.

11. Daigle, B. Printed circuit board material and design considerations for wireless applications. In Proceedings of the 46th Electronic Components and Technology Conference, Orlando, FL, USA, 28–31 May 1996; pp. 354–357.

12. Chen, Q.; Gong, Z.; Yang, X.; Wang, Z.; Zhang, L. Design considerations for millimeter wave antennas within a chip package. In Proceedings of the IEEE International Workshop on Anti-Counterfeiting, Security and Identification, Xiamen, China, 16–18 April 2007; pp. 13–17.

13. Nielsen, J.Ø.; Pedersen, G.F. Performance of Beamforming for a Handheld Device in Measured 21.5 GHz Indoor Channels. *IEEE Trans. Antennas Propag.* **2022**, *70*, 5725–5735. [CrossRef]

14. Sani Yahya, M.; Rahim, S. 15 GHz grid array antenna for 5G mobile communications system. *Microw. Opt. Technol. Lett.* **2016**, *58*, 2977–2980. [CrossRef]

15. Helander, J.; Zhao, K.; Ying, Z.; Sjöberg, D. Performance Analysis of Millimeter-Wave Phased Array Antennas in Cellular Handsets. *IEEE Antennas Wirel. Propag. Lett.* **2016**, *15*, 504–507. [CrossRef]

16. Sun, W.; Li, Y.; Chang, L.; Li, H.; Qin, X.; Wang, H. Dual-band dualpolarized microstrip antenna array using double-layer gridded patches for 5G millimeter-wave applications. *IEEE Trans. Antennas Propag.* **2021**, *69*, 6489–6499. [CrossRef]

17. Seo, J.; Yoon, I.; Jung, J.; Ryoo, J.; Park, J.; Lee, W.; Ko, D.; Oh, J. Miniaturized dual-band broadside/endfire antenna-in-package for 5G smartphone. *IEEE Trans. Antennas Propag.* **2021**, *69*, 8100–8114. [CrossRef]

18. Ojaroudi, N.; Ghadimi, N. UWB small slot antenna with WLAN frequency band-stop function. *Electron. Lett.* **2013**, *49*, 1317–1318. [CrossRef]

19. Sethi, W.T.; Vettikalladi, H.; Minhas, B.K.; Alkanhal, M.A. High gain and wide-band aperture-coupled microstrip patch antenna with mounted horn integrated on FR4 for 60 GHz communication systems. In Proceedings of the IEEE Symposium on Wireless Technology and Applications (ISWTA), Kuching, Malaysia, 22–25 September 2013; pp. 359–362.

20. Hong, W.; Baek, K.; Lee, Y.; Kim, Y.G. Design and analysis of a low-profile 28 GHz beam steering antenna solution for future 5G cellular applications. In Proceedings of the IEEE International Microwave Symposium, Tampa, FL, USA, 1–6 June 2014.

21. Salman, J.W.; Ameen, M.M.; Hassan, S.O. Effects of the loss tangent, dielectric substrate permittivity and thickness on the performance of circular microstrip antennas. *J. Eng. Dev.* **2006**, *10*, 1–13.

22. Salokhe, B.T.; Mali, S.N. Effect of substrate material variations on RMSA, CMSA and NLMSA. *Int. J. Adv. Res. Electr. Electron. Instrum. Eng.* **2014**, *3*, 14009–14015.

23. *CST Microwave Studio*, Version 2020; CST: Framingham, MA, USA, 2020.

24. Amitay, N.; Galindo, V.; Wu, C.P. *Theory and Analysis of Phased Array Antennas*; Wiley-Interscience: New York, NY, USA, 1972.

25. Xu, R.; Chen, Z.N. A Compact Beamsteering Metasurface Lens Array Antenna with Low-Cost Phased Array. *IEEE Trans. Antennas Propag.* **2021**, *69*, 1992–2002. [CrossRef]

26. Guo, J.; Xiao, S.; Liao, S. A Low-Cost Feeding Network with Simple Phase Shift Structures. In Proceedings of the 2018 IEEE International Conference on Computational Electromagnetics (ICCEM), Chengdu, China, 26–28 March 2018; pp. 1–3.

27. Roshani, S.; Koziel, S.; Roshani, S.; Jamshidi, M.B.; Parandin, F.; Szczepanski, S. Design of a Patch Power Divider with Simple Structure and Ultra-Broadband Harmonics Suppression. *IEEE Access* **2021**, *9*, 165734–165744. [CrossRef]

28. Parchin, N.O. Dual-Band Phased Array 5G Mobile-Phone Antenna with Switchable and Hemispherical Beam Pattern Coverage for MIMO-Diversity Communications. *ACES J.* **2022**, *36*, 1602–1609. [CrossRef]

29. Nakano, H.; Yamauchi, J. Printed slot and wire antennas: A Review. *Proc. IEEE* **2012**, *100*, 2158–2168. [CrossRef]

30. Kim, D.-Y.; Lim, Y.; Yoon, H.-S.; Nam, S. High-Efficiency W-Band Electroforming Slot Array Antenna. *IEEE Trans. Antennas Propag.* **2015**, *63*, 1854–1857. [CrossRef]

31. Ojaroudi, N. Application of protruded strip resonators to design an UWB slot antenna with WLAN band-notched characteristic. *Prog. Electromagn. Res. C* **2014**, *47*, 111–117. [CrossRef]

32. Hong, W.; Ko, S.-T.; Lee, Y.; Baek, K.-H. Compact 28 GHz antenna array with full polarization flexibility under yaw, pitch, roll motions. In Proceedings of the 2015 9th European Conference on Antennas and Propagation (EuCAP), Lisbon, Portugal, 13–17 April 2015; pp. 1–3.

33. Available online: https://www.lasercalculator.com/db-percent-converter/ (accessed on 14 September 2022).

34. Hong, W.; Baek, K.-H.; Ko, S. Millimeter-wave 5G antennas for smartphones: Overview and experimental demonstration. *IEEE Trans. Antennas Propag.* **2017**, *65*, 6250–6261. [CrossRef]

35. Ide, T.; Kanaya, H. 28 GHz one-sided directional slot array antenna for 5G application. In Proceedings of the 2019 IEEE 21st Electronics Packaging Technology Conference (EPTC), Singapore, 4–6 December 2019; pp. 440–443.

36. Chen, C.-N.; Lin, Y.-H.; Hung, L.-C.; Tang, T.-C.; Chao, W.-P.; Chen, C.-Y.; Chuang, P.-H.; Lin, G.-Y.; Liao, W.-J.; Nien, Y.H. 38-GHz Phased Array Transmitter and Receiver Based on Scalable Phased Array Modules with Endfire Antenna Arrays for 5G MMW Data Links. *IEEE Trans. Microw. Theory Tech.* **2021**, *69*, 980–999. [CrossRef]

37. Ojaroudiparchin, N.; Shen, M.; Pedersen, G.F. Beam-steerable microstrip-fed bow-tie antenna array for fifth generation cellular communications. In Proceedings of the 2016 10th European Conference on Antennas and Propagation (EuCAP), Davos, Switzerland, 10–15 April 2016.

38. Zhang, J.; Zhang, S.; Li, Y.; Pedersen, G.F. Printed vertically- polarized quasi-endfire beam steering array with full ground plane for 5g mobile applications. In Proceedings of the 13th European Conference on Antennas and Propagation (EuCAP), Krakow, Poland, 31 March–5 April 2019.

39. Ojaroudiparchin, N.; Shen, M.; Zhang, S.; Pedersen, G.F. A switchable 3-D-coverage-phased array antenna package for 5G mobile terminals. *IEEE Antennas Wirel. Propag. Lett.* **2016**, *15*, 1747–1750. [CrossRef]

40. Zhang, J.; Zhang, S.; Lin, X.; Fan, Y.; Pedersen, G. 3D radiation pattern reconfigurable phased array for transmission angle sensing in 5G mobile communication. *Sensors* **2018**, *18*, 4204. [CrossRef] [PubMed]

41. Parchin, N.O.; Shen, M.; Pedersen, G.F. Small-size tapered slot antenna (TSA) design for use in 5G phased array applications. *Appl. Comput. Electromagn. Soc. (ACES) J.* **2017**, *3*, 1054–4887.

42. Zhao, A.; Ai, F. 5G mm-wave antenna array based on T-slot antenna for mobile terminals. In Proceedings of the 2018 IEEE Asia-Pacific Conference on Antennas and Propagation (APCAP), Auckland, New Zealand, 5–8 August 2018.

43. Ojaroudi Parchin, N.; Al-Yasir, Y.; Abdulkhaleq, A.M.; Elfergani, I.; Rayit, A.; Noras, J.M.; Rodriguez, J.; Abd-Alhameed, R.A. Frequency reconfigurable antenna array for mm-Wave 5G mobile handsets. In Proceedings of the 9th International Conference on Broadband Communications, Networks, and Systems, Faro, Portugal, 19–20 September 2018.

44. Tatomirescu, A.; Oprian, A.; Zhekov, S.; Pedersen, G.F. Beam-steering array for handheld devices targeting 5G. In Proceedings of the 2015 International Symposium on Antennas and Propagation (ISAP), Hobart, TAS, Australia, 9–12 November 2015.

45. Park, E.; Yoon, Y.J.; Kim, H. Dual Polarization L-Shaped Slot Array Antenna for 5G Metal-Rimmed Mobile Phone. In Proceedings of the 2018 International Symposium on Antennas and Propagation (ISAP), Busan, Korea, 23–26 October 2018; pp. 1–2.

46. Rafique, U.; Dalal, P.; Abbas, S.M.; Khan, S. Phased Array Antenna for Millimeter-Wave 5G Mobile Phone Applications. In Proceedings of the 2022 IEEE Wireless Antenna and Microwave Symposium (WAMS), Rourkela, India, 5–8 June 2022; pp. 1–4. [CrossRef]

47. di Paola, C.; Zhao, K.; Zhang, S.; Pedersen, G.F. Hybrid Switchable Phased Array with p-i-n Diodes for 5G Mobile Terminals. In Proceedings of the 2021 15th European Conference on Antennas and Propagation (EuCAP), Dusseldorf, Germany, 22–26 March 2021; pp. 1–5. [CrossRef]

48. Parchin, N.O.; Zhang, J.; Abd-Alhameed, R.A.; Pedersen, G.F.; Zhang, S. A planar dual-polarized phased array with broad bandwidth and quasi-endfire radiation for 5G mobile handsets. *IEEE Trans. Antennas Propag.* **2021**, *69*, 6410–6419. [CrossRef]

49. Ilvonen, J.; Kivekas, O.; Holopainen, J.; Valkonen, R.; Rasilainen, K.; Vainikainen, P. Mobile terminal antenna performance with the user's hand. *IEEE Antenna Wirel. Propag. Lett.* **2011**, *10*, 772–775. [CrossRef]

50. Alshamaileh, M.H.; Alja'afreh, S.S.; Almajali, E. Nona-band, hybrid antenna for metal-rimmed smartphone applications. *IET Microw. Antennas Propag.* **2019**, *13*, 2439–2448. [CrossRef]